Structurally and mechanically tunable molybdenum oxide films and patterned submicrometer structures by electrodeposition

A. Quintana[1], A. Varea[1,2*] *avarea@el.ub.edu,* M. Guerrero[1], S. Suriñach[1], M. D. Baró[1], J. Sort[3#] *jordi.sort@uab.cat,* E. Pellicer[1§] *eva.pellicer@uab.cat*

[1] *Departament de Física, Facultat de Ciències, Universitat Autònoma de Barcelona, E-08193 Bellaterra, Spain.*

[2] *Departament d'Electrònica, Facultat de Física, Universitat de Barcelona, C/ Martí i Franquès 1, E-08028, Barcelona, Spain.*

[3] *Institució Catalana de Recerca i Estudis Avançats (ICREA) and Departament de Física, Universitat Autònoma de Barcelona, E-08193 Bellaterra, Spain.*

*[#§] *Corresponding authors.*

This is the author's version of a work that was accepted for publication in Electrochimica acta (Elsevier). Changes resulting from the publishing process, such as peer review, editing, corrections, structural formatting, and other quality control mechanisms may not be reflected in this document. Changes may have been made to this work since it was submitted for publication. A definitive version was subsequently published in Quintana, A. et al. "Structurally and mechanically tunable molybdenum oxide films and patterned submicrometer structures by electrodeposition", Electrochimica Acta, vol. 173, Aug. 2015, p.705–714. This is the author's version of a work that was accepted for publication in Electrochimica acta (Elsevier). DOI 10.1016/j.electacta.2015.05.112

Graphical Abstract

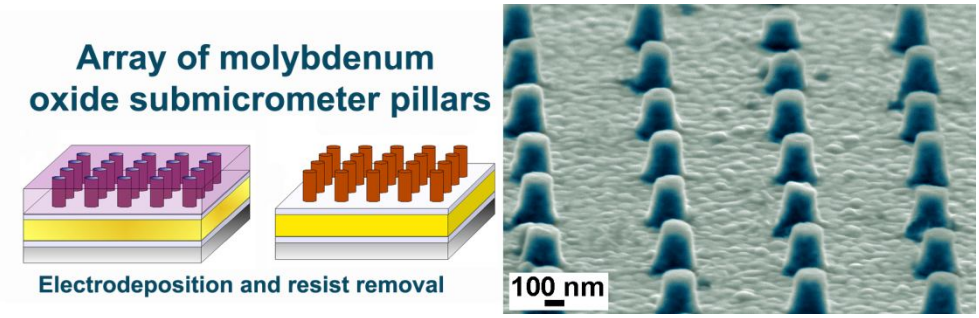

Abstract

1.5 μm-thick molybdenum oxide films have been electrodeposited potentiostatically from 0.2 M Na_2MoO_4 electrolyte onto indium tin oxide (ITO)/glass substrates at pH = 1, 6 and 9. The influence of cetyltrimethylammonium bromide (CTAB) surfactant on films' adhesion, morphology, degree of porosity, molybdenum speciation, and crystallographic structure has been systematically investigated. The addition of CTAB (0.01 M) to the bath clearly improves film adherence to the substrate, reduces cracking, and increases crystallinity. This has an impact on the physical properties of the films. In particular, both hardness (*H*) and Young's modulus (*E*) increase, as determined from nanoindentation tests. The growth of ordered arrays of molybdenum oxide submicrometer structures, including pillars and stripes, by electrodeposition onto e-beam lithographed Au/Ti/Si substrates is also reported.

Keywords: molybdenum oxide; electrodeposition; cationic surfactant; X-ray diffraction; mechanical properties.

1. Introduction

Transition metal oxides in thin-film form have received much attention owing to their promising applications in electrochromics, energy storage, sensing, and non-volatile resistive random access memory devices, among others [1-3]. Molybdenum oxide is a suitable candidate in many of these applications due to its unusual chemistry produced by multiple Mo valence states (IV, V and VI) and a rich variety of crystallographic structures [3,4]. MoO_2, with its distorted rutile structure, presents a high metal-like conductivity [5] and it finds uses as anode material in solid oxide fuel cells [6]. In addition, its layered structure makes it suitable as ion intercalation/deintercalation host in, for instance, lithium batteries [3,7]. MoO_3 is an n-type semiconductor with two most common crystal phases: the thermodynamically stable orthorhombic α-MoO_3 and the metastable monoclinic β-MoO_3, that show optical switching upon thermal, photo (photochromism) [8-10] or electric (electrochromism) [11,12] excitations. Such an optical modulation (colouration/bleaching) is effectively used in many applications like smart windows and antidazzling coatings [13]. The crystallinity degree is an important asset depending on the end application. For example, amorphous molybdenum oxide is suitable as an electrochemical sensor for iodate ions [14], whereas MoO_3 nanocrystalline films and nanorods can serve as gas sensors toward H_2 [15] and NO_2 [16], respectively. In addition, nanostructured α-MoO_3 has been applied as supercapacitor electrodes in acid aqueous electrolytes [17]. For all these reasons, controlling both the valence state and the crystallographic structure of the molybdenum oxide materials is of prime importance to meet the required technological demands.

So far, molybdenum oxides have been prepared by a variety of physical and chemical techniques: pulsed laser deposition [18], chemical vapour deposition [19], sputtering [20], thermal evaporation [21], spray pyrolysis [22], electrodeposition [23,24], anodization [25], and sol-gel [26]. Electrochemical methods are advantageous for several reasons. They are

generally easy to perform and can be readily used to tailor films' properties. In particular, electrodeposition offers facile control over thickness, morphology, extent of oxidation and doping of the films at ambient pressure. The influence of bath formulation and growth conditions on the oxidation state of molybdenum oxide films has been studied in detail in the past [3]. McEvoy and Stevenson described the cathodic electrodeposition of MoO_3 from acidic peroxo-polymolybdate solutions onto indium-doped tin oxide (ITO) electrode [27]. The same authors deeply investigated the mechanism of molybdenum oxides deposition using different tools, namely chronocoulometry and quartz crystal microbalance techniques [28,29]. The authors showed that a graded reduction of molybdenum precursors toward amorphous hydrates of non-stoichiometric, mixed-valent molybdenum oxides takes place from acidic peroxo-polymolybdate solutions. Patil et al. explored the electrosynthesis of hydrous amorphous MoO_2 thin films from an alkaline solution containing ammonium molybdate (pH = 9) [11]. Layered films consisting of mostly Mo(IV) were obtained from citrate-molybdate solutions at pH = 8.3 by applying different potentials [23]. The potentiostatic deposition of molybdenum oxides with mixed valence states of Mo(V) and Mo(IV) was also described in citrate-molybdate electrolytes at pH = 6.6 [30]. From literature screening, it is evident that bath pH is a key parameter in determining the Mo oxidation state in the films. Nevertheless, other parameters also have an effect on the oxidation state of electrodeposited molybdenum oxide, such as the deposition technique. For example, it was found that MoO_3 films deposited at pH = 1 by cyclic voltammetry contained a mixture of Mo^{V} and Mo^{VI} and were less homogeneous than those obtained potentiostatically, for which only Mo^{VI} was detected [31]. Also, the crystallinity and phases obtained are very sensitive to the electrodeposition conditions. It was found that the sweep rate in cyclic voltammetry experiments determined the formation of either α- or β-MoO_3 [24]. Remarkably, X-ray diffraction analyses indicate that the films are typically

amorphous (or poorly crystalline) in the as-deposited state [11,24,27]. Therefore, annealing at temperatures equal to (or beyond) 250 ºC is typically required to achieve fully crystalline films [11,27]. Guerfi et al. [32] showed that an increase in crystallinity of the as-deposited molybdenum oxide is possible after heat-treating the films in air at 260 ºC and that complete crystallization occurs at 300ºC.

In order to favour the growth of fully crystalline molybdenum oxide deposits without the need for a heat-treatment, additives can be added to the bath. Additives usually play an important role in electrodeposition processes as they bring or change some microstructural features of electrodeposited materials. Cetyltrimethylammonium bromide (CTAB) is a cationic surfactant widely used in electrodeposition. In particular, it is known to be a corrosion inhibitor [33] and grain refiner [34] in metals electrodeposition. Also, it is used as templating agent for the electrochemical production of metal oxide foams [35,36]. Thus, it is envisaged that the addition of CTAB to the electrolyte could impact molybdenum oxide film growth and, in turn, modulate molybdenum oxidation state, crystallographic structure, film adhesion, and porosity.

In spite of numerous studies paying attention to the physicochemical properties and applications of molybdenum oxides, only few works have investigated their mechanical properties [37] and, to the best of our knowledge, none of them are related to the mechanical behaviour of electrodeposited molybdenum oxide films. Actually, since the adherence of electrodeposited molybdenum oxide films to the substrate is poor or either the layers feature cracks, the measurement of their mechanical properties by micro- or nanoindentation is certainly not straightforward. This has probably precluded any detailed study in the field.

With the continuing trend toward miniaturization of devices, electrodeposition has been typically combined with polycarbonate/aluminum oxide membranes and e-beam

lithographed substrates to obtain patterned arrays of nanostructures. Ordered arrays of Mo oxide nanowires have been recently produced by Inguanta and co-workers on commercial track-etched polycarbonate membranes [38]. Examples of patterned nanostructures obtained by electrodeposition on e-beam lithographed substrates can be found in the literature, especially for magnetic metals and alloys [39]. However, there is a dearth of literature on template-assisted electrodeposition of metal oxides on pre-patterned substrates.

In this work, molybdenum oxide films have been potentiostatically deposited onto ITO/glass substrates and the effect of CTAB additive onto films' morphology and structure at three different pH values has been explored. Our results reveal that CTAB improves the adherence of the deposits to the substrate and thus consistently facilitates the measurement of relevant mechanical parameters, like hardness or Young's modulus, by means of nanoindentation. Furthermore, the preparation of ordered arrays of molybdenum oxide submicrometer structures –pillars and stripes– by template-assisted electrodeposition is presented.

2. Experimental techniques

Molybdenum oxide films were obtained potentiostatically by direct current electrodeposition in one-compartment thermostatized three-electrode cell using a PGSTAT120N Autolab potentiostat/galvanostat (Ecochemie). ITO-coated glass (surface resistivity 30-60 Ω/sq.) was used as working electrode (WE) in both cyclic voltammetry (CV) experiments and potentiostatic deposition. In all cases the WE was positioned vertically within the electrolyte. The working area was set between 0.2 and 0.4 cm^2. A Ag|AgCl (3M KCl) (E=+0.210 V versus standard hydrogen electrode (SHE)) reference electrode (Metrohm AG) was used. A platinum sheet served as the counter electrode.

Molybdenum oxide films were deposited from an electrolyte containing either 0.2 M $Na_2MoO_4 \cdot 2H_2O$ (labeled as "no add" bath) or 0.2 M $Na_2MoO_4 \cdot 2H_2O$ + 0.01 M $C_{19}H_{42}BrN$ (labeled as "CTAB" bath). The electrolyte volume was 50 mL. Analytical grade reagents and ultrapure water (18 MΩ cm) were used to prepare the plating solution. The pH values selected were 1, 6 and 9. The pH was adjusted with either H_2SO_4 or NaOH. Potentiostatic deposition was applied under mild stirring (100 rpm) using a magnetic stirrer bar. The temperature of the bath was set at 25°C. The electrical charge was adjusted across all depositions to attain similar film thicknesses (approximately 1.5 μm). Prior to deposition, the ITO surface was first degreased with acetone and later rinsed with ultrapure water. Before and during each deposition, the electrolyte was deaerated with argon gas flow.

For the growth of ordered arrays of molybdenum oxide submicrometer structures, e-beam patterned Au/Ti/Si substrates were used as the cathode. First, Ti (100 nm)/Au (400 nm)/Ti (15 nm) were evaporated onto Si(111) substrates. An electron sensitive resist (ZEP-520A) of about 500 nm in thickness was then spin-coated onto the substrate and patterning was carried out by electron-beam lithography (EBL) with the CRESTEC CABL-9500C electron-beam lithography machine. Arrays of cylindrical holes of 200 nm and 500 nm in diameter and stripes of 100 nm, 500 nm and 1 μm width (15 μm lengths) were patterned. Following the lithographic procedure, the resist was developed in anisol. Before electrodeposition, all samples were submerged in HF solution for 1 min to remove the upper 15 nm-thick Ti layer to allow the deposition of molybdenum oxide directly onto the Au surface. Finally, the substrates were dipped in diluted sulphuric acid to remove oxides and organic residues. The Au/Ti/Si substrates were then immersed in the electrolyte for 10 min before deposition was started. After electrodeposition, the resist was etched with dimethylacetamide at 35 °C for 1 min.

The morphology of the deposits was examined by field emission scanning electron microscopy (FE-SEM) using a Zeiss MERLIN microscope operated at 1.2 kV to prevent from charging effects. Energy dispersive X-ray (EDX) analyses were carried out at 15 kV. The crystallographic structure of the films was studied by X-ray diffraction (XRD). XRD patterns were recorded on a Philips X'Pert diffractometer using the Cu K_α radiation, in the 10°–70° 2θ range (0.03° step size, 10 s holding time). Complementary transmission electron microscopy (TEM) observations were carried out on a Jeol-JEM 2011 system operated at 200 kV. The films were subjected to ultrasonication for 10 min in isopropyl alcohol and then a couple of drops of the suspension were placed dropwise onto a carbon-coated Cu TEM grid. X-ray photoelectron spectroscopy (XPS) analyses were carried out on a PHI 5500 Multitechnique System (from Physical Electronics) spectrometer, equipped with a monochromatic X-ray source ($K_{\alpha Al}$ line with energy of 1486.6 eV and 350 W), placed perpendicular to the analyser axis and calibrated using $3d^{5/2}$ line of Ag with a full width at half maximum (FWHM) of 0.8 eV. The analysed area was a 0.8 mm diameter disk surface for each sample. Charging effects were corrected by referencing the binding energies to that of the adventitious Cls line at 284.5 eV. Linear background was assumed [40]. The Mo3d peaks were deconvoluted assuming Gaussian functions. The energy of the deconvoluted peaks was compared with the NIST XPS database [41].

The mechanical properties of the films, hardness (H) and reduced Young modulus (E_r), were evaluated by nanoindentation in the load control mode, using an UMIS device from Fischer-Cripps Laboratories equipped with a Berkovich pyramidal-shaped diamond tip. The maximum applied force was 0.2 mN to ensure that the maximum penetration depth during the tests was kept below 10% of the overall film thickness. Thermal drift during the nanoindentation tests was kept below 0.05 nm s^{-1}. Corrections for the contact area (calibrated with a fused quartz specimen), instrument compliance, and initial penetration

depth were applied. H and E_r were derived from the load-displacement curves at the beginning of the unloading segment using the method of Oliver and Pharr [42]. Data reported corresponds to the averaging of 60 indentations per sample. *H* and E_r were also determined for the molybdenum oxide stripes (with a thickness of 500 μm). The maximum applied force was also chosen to be 0.2 mN.

3. Results and Discussion

3.1. Molybdenum oxide films deposition

Prior to the preparation of the films, the main features of molybdenum oxides deposition from Mo(VI) baths on ITO/glass substrate were studied by CV both without and with CTAB in the bath (Figure 1). In all cases the potential was scanned from –0.1 V toward negative values and then reversed toward the positive direction, at scan rate of 50 mV s^{-1}. In CTAB-free baths, the detection of negative current was progressively shifted toward more positive potentials as the pH of the bath decreased, in agreement with other works [24, 30]. A diffusion-controlled like peak was observed at pH = 1 and more clearly at pH = 6. A broad and asymmetric oxidation peak centered at –0.3 V was recorded at pH = 6 both with and without CTAB. This peak is likely attributed to oxidation of molecular hydrogen formed during the reduction process. Molybdenum oxides are known to catalyze the hydrogen evolution reaction [43]. Small differences were observed depending on whether CTAB was absent or present in the bath, but the main features of the CV were maintained at each pH value. From the CV data, it was decided to deposit molybdenum oxide films at a potential of –1.4 V from baths at pH = 6 and pH = 9, and at a potential of –0.9 V from the bath at pH = 1 in order to avoid excessive hydrogen co-evolution. It should be noted that these values are much more negative than those typically reported in the literature for the potentiostatic deposition

of molybdenum oxides [23,30,31]. However, as it will be shown later, adherent and crystalline molybdenum oxide films can be produced at such potentials in CTAB-containing baths. It should be noticed that the CTAB-containing solution at pH = 1 was not stable. When CTAB was added to the bath, a whitish precipitate appeared. Molybdic acid aggreates are formed upon reaction of ammonium molybdate in acidic media containing CTAB [44]. For this reason, this solution was not considered for the subsequent preparation of molybdenum oxide films.

Figure 2 shows the *j*-t curves recorded during the growth of the molybdenum oxide films at different pH with and without CTAB in the bath. Interestingly, the *j*-t curve corresponding to the CTAB-free bath at pH = 1 shows a peculiar and reproducible behaviour; the current is kept constant at –2.7 mA cm^{-2} for almost 250 s and then suddenly drops toward less negative values. The electrolyte turned blue but remained transparent soon after the ITO substrate became covered by a blue film, indicating that there was a competition between deposition and partial dissolution of the growing film. A transparent dark blue film was obtained at the end of deposition. The solution could not be re-used in subsequent depositions since no deposit formation was further detected on the substrate under the same conditions (applied potential and time). The *j*-t curves recorded from the other baths (pH = 6 and pH = 9) display a different profile. Namely, a less or more pronounced maximum in the *j*-t curve is achieved soon after the potential is applied followed by a relaxation of the current toward more positive values (see inset of Figure 2). At each pH, more negative current densities were recorded in CTAB-free baths, likely because CTAB exerts some effect on the electrochemical double layer. Brown and dark brown films were obtained at pH = 6 and pH = 9, respectively, irrespective of whether CTAB was present or not in the bath. A metallic

luster was noticed at the film/ITO interface when looking at these samples from the backside.

3.2 Morphological and structural characterization of molybdenum oxide films

SEM images of the films revealed the occurrence of cracks throughout the surface, especially in films produced from CTAB-free baths (Figure 3a, 3b and 3d). The formation of cracks and their propagation was partly due or at least enhanced by the vacuum conditions of the SEM microscope. Delamination of the film was also observed in some regions. These phenomena were noticed in real time while visualizing the samples by SEM. This suggests that the as-deposited films are highly stressed and that this stress is relieved in the form of cracks and delamination when vacuum is applied. Nevertheless, this cracked surface has been observed many times in the literature, even for lower thicknesses [11,30]. Cracking has been attributed to the drying shrinkage of hydrous oxide films whose thickness is greater than 0.2 µm [11]. The sample obtained from CTAB-free bath at pH 1 (Figure 3a) is highly porous, which further confirms the occurrence of intensive hydrogen co-evolution during film growth. CTAB has a positive effect on cracking phenomena. Namely more adherent and less cracked films are obtained in the presence of CTAB in the bath (Figures 3c and 3e). It is worth mentioning that the selected CTAB concentration is rather optimal. For example, films deposited at pH = 9 with 0.001 M CTAB featured wider cracks between plates than films deposited with 0.01 M CTAB. A reduction of the crack width was noticed upon increasing the CTAB concentration. Fewer cracks, smaller crack widths and best film adhesion were indeed observed for 0.01 M CTAB. Further increase of the CTAB

concentration up to 0.1 M again increased crack density compared to 0.01 M CTAB. Interestingly, the film obtained at pH = 6 from the CTAB-containing bath is also highly porous compared to its CTAB-free analogue (cf. Figures 3c and 3b). This result indicates that CTAB is a convenient templating agent for the production of 3D molybdenum oxide foams at moderate pH values [35,36], which could be of interest in applications such as anode for lithium-ion batteries or electrocatalysis.

X-ray diffraction analysis of the deposited films was carried out in order to determine their crystallinity degree and the phases present. As aforementioned, the deposition charge was adjusted in each case so that films of similar thickness (ca. 1.5 μm) were achieved. The corresponding diffractograms indicate that the films are composed of up to four crystalline phases: orthorhombic α-MoO_3, hydrated $MoO_3 \cdot H_2O$, and substoichiometric Mo_xO_{3x-1} (i.e. Mo_8O_{23} and Mo_4O_{11}) phases (Figure 4). By lowering the ratio of oxygen to Mo content down to 2.9 and below, metastable suboxides like Mo_8O_{23} and Mo_4O_{11} can form. Notice that in Mo_4O_{11}, the oxidation state of Mo is +5. Hence, this compound can be described as a double Mo_2O_5 molecule coordinated via one oxygen atom [23]. In addition, an amorphous background located between 40º and 50º is detected in all diffractograms, being more or less prominent depending on the deposition conditions. The hump centered at 2θ = 25º arises from the glass/ITO substrate. All the reflections in the film obtained from the CTAB-free bath at pH = 1 (Figure 4a) can be assigned to substoichimetric Mo_xO_{3x-1}. Thinner (4-10 nm) films obtained potentiostatically at pH = 1 from 0.2 M MoO_4^{2-} bath were shown to consist of two oxidation states, Mo^V and Mo^{VI}, by XPS [31]. Bluish molybdenum oxide films have been linked to Mo^{VI}/Mo^V, whereas brown-violet films have been typically ascribed to more reduced molybdenum oxides ($Mo^{VI}/Mo^V/Mo^{IV}$) [28]. At pH = 6 (Figure 4b), α-MoO_3 is the most abundant phase in the film deposited from CTAB-containing bath,

whereas the most intense reflections in the film deposited from CTAB-free solution match again substoichimetric Mo_xO_{3x-1} compounds. Mo_4O_{11} films were also obtained by electrodeposition on stainless steel from 0.25 M ammonium molybdate (pH = 6.5–7.0) at current densities ranging from –3.5 to –7 mA cm^{-2} [45]. Finally, α-MoO_3 also clearly predominates in the film deposited from CTAB-containing bath at pH = 9. Moreover, the α-MoO_3 phase is strongly textured in the (020) plane (2θ = 12.8º) in CTAB films produced at pH = 6 and pH = 9. Much less intense reflections ascribed to hydrated MoO_3 and substroichiometric Mo_xO_{3x-1} are also identified in the diffractogram corresponding to the sample produced from CTAB-containing bath at pH = 9. Contrarily, a rather amorphous film is obtained when CTAB is not present in the bath. This is consistent with the work from Patil et al., who obtained a fully amorphous film by potentiostatic deposition onto F-doped SnO_2 (FTO) from an ammonium molybdate bath at pH = 9 [11]. In our case, only very weak reflections superimposed to the amorphous background are identified. The obtained results suggest that CTAB significantly improves the crystallinity of the deposits, particularly at pH = 9.

It should be noted that, compared to most of the previous works, the molybdenum oxide films are partly crystalline already in the as-deposited state. This can be in part ascribed to the larger thickness of the here-prepared films (1.5 μm) as compared to the nanometer-thick films typically reported in the literature on ITO and FTO substrates. For example, McEvoy et al. prepared films of 100-200 nm in thickness [27] and Gacicuta et al. prepared films between 4 nm to 10 nm in thickness [31], both on ITO substrates. Likewise, Patil et al. obtained films ranging from 274 nm to 604 nm on FTO substrates [11]. The structure of the film during nucleation and initial growth stages is highly influenced by the substrate nature. Since glass/ITO is mostly amorphous, the first layers tend to grow in the amorphous state. At longer deposition times, the structure of

the deposit is no longer influenced by the substrate, but depends only on the electrodeposition conditions [46].

Molybdenum oxide films were also subjected to TEM characterization. Figure 5 shows representative high-resolution TEM images and corresponding selected area electron diffraction (SAED) patterns for some films. The interplanar distances match the phases previously encountered in XRD analyses.

X-ray photoelectron spectroscopy (XPS) analyses were further conducted in order to get a deeper knowledge of the speciation of Mo compounds in the different films. Figure 6 and Figure 7 show the experimental and deconvoluted Mo3d core electronic transitions for the films obtained without and with CTAB in the bath, respectively. Deconvolution was performed using 100% Gaussian functions. Table 1 lists the energies of the deconvoluted peaks for the CTAB-free films. The presence of Mo^{VI} and Mo^{V} was confirmed in all cases. Additionally, Mo^{IV} and Mo^{0} were also detected. Their relative abundance varied depending on both the pH and the presence of CTAB in the bath. Some general trends can be drawn. At pH = 1, Mo^{V} state is predominant (Figure 6a), in agreement with XRD analyses and previous works in the literature [28,31]. The spectra also indicate the existence of Mo^{VI} and Mo^{IV} oxidation states. Although the detection of Mo^{IV} at such low pH is uncommon, it is also true that the here-prepared films are relatively thick. In other words, thickness might also play a role on the evolution of molybdenum oxidation states. Mo^{VI} and Mo^{V} are predominant in films obtained at pH = 6 from CTAB-free bath (Figure 6b). The detection of Mo^{V} is consistent with XRD analysis. However, the XRD pattern does not show peaks attributed to α-MoO_3 or any other Mo(VI) species, whereas XPS peak deconvolution indicate that Mo^{VI} is present. This suggests that either Mo(VI) species are amorphous or partial oxidation of substoichiometric Mo_xO_{3x-1} toward Mo(VI) species at the utmost surface occurred. The

latter hypothesis seems more reasonable taking into account the brownish coloring, typical of reduced molybdenum oxide, of the deposit [23,30]. Bear in mind that X-rays penetrate deeper in the film, while only the utmost surface is explored by XPS. Additionally, Mo^{IV} is also relatively abundant in the homologous CTAB film (Figure 7a). Since no diffraction peaks ascribed to MoO_2 are present in the corresponding diffractogram, this would indicate that Mo(IV) species are amorphous. Indeed, the presence of reduced molybdenum oxides at quasi-neutral pH and higher has been widely reported in the literature [23,30]. Finally, Mo^{VI} and Mo^{V} are the prevalent oxidation states at pH = 9 with and without CTAB. Since no peaks ascribed to Mo(VI) compounds are detected in the XRD pattern of the CTAB-free bath this might again suggest that Mo_xO_{3x-1} underwent oxidation at the surface. Interestingly, the relative amount of Mo^{IV} is higher in the film obtained from CTAB-free bath (cf. Figure 6c – shoulder ca. 229.8 eV– and Figure 7b). The results gleaned from XPS indicate that the addition of CTAB to the bath induces changes in the speciation of Mo compounds. In particular, the presence of CTAB in the electrolyte at pH = 9 seemingly favors the growth of less reduced molybdenum oxides. Finally, the detection of metallic molybdenum was quite surprising since it is believed that complete reduction of Mo(VI) toward Mo(0) from aqueous baths requires the presence of an inductor cation in solution (e.g. Co, Ni, Fe) and hydroxycarboxylic acids, which is not our case. However, Morley et al. succeeded in the deposition of metallic molybdenum from acetate-rich aqueous electrolytes [47]. It is believed that metallic Mo is formed during the first stages of deposition. It is conjectured that metallic Mo is not detected by XRD because either its relative amount in the overall film thickness is below the detection limit of the XRD technique (which is usually taken as 1-2 wt%), or the signal is masked by the amorphous background. As aforementioned, a metallic luster was seen from the

backside of ITO/glass substrate. Because the layers feature some cracks, Mo^0 could be detected by XPS although it is likely located at the substrate/film interface.

3.3. Mechanical properties of molybdenum oxide films

The nanoindentation curves of the different molybdenum oxide films are plotted in Figure 8. The penetration depth reached at the end of the indentation segment varies depending on both the pH of the bath and the absence/presence of CTAB. This, in turn, means that hardness, H, and reduced Young's modulus, E_r, are sensitive to the Mo oxidation state, crystallographic structure, and porosity of the films. Table 2 lists the values of H and E_r for the different films. In particular, the presence of CTAB in the bath leads to mechanically harder films. This is in part due to the decrease in the amount of cracks. The hardest film is the one produced from CTAB-containing bath at pH = 9, whereas the softest film stands for its CTAB-free homologous, which is almost fully amorphous (Figure 4c). Note that not only H increases when CTAB is added to the bath, but also E_r does. It is well known that amorphous oxides tend to be mechanically softer than crystalline ones [48]. The real Young's modulus (E) has been calculated by using the following equation:

$$\frac{1}{E_r} = \frac{1-\nu^2}{E} - \frac{1-\nu_i^2}{E_i} \qquad (1)$$

where E_i = 1140 GPa and ν_i = 0.07 stand for diamond indenter. A Poisson's ration ν = 0.28 has been assumed for molybdenum oxide [49]. The obtained E values are much lower than those of bulk MoO_3 (E_{bulk} = 540 GPa) [50]. Such a decrease in the Young's

modulus can be explained by taking the presence of cracks and porosity into account. The porosity fraction (*P*) has been estimated from equation (2) [51]:

$$\frac{E}{E_{bulk}} = \frac{(1-p)^2}{1+2p-3\nu p} \qquad (2)$$

where E is the Young's modulus of the material under investigation and E_{bulk} the Young's modulus of the bulk, and from equation (3, 4) [52]:

$$\frac{E}{E_{bulk}} = C_1\left(\frac{\rho}{\rho_{bulk}}\right)^2 \qquad (3)$$

$$P(\%) = 1 - \frac{\rho}{\rho_{bulk}} \times 100 \qquad (4)$$

where C_1 is a geometric constant close to 1 and ρ/ρ_{bulk} the relative density of the material under study. The resulting values of porosity (*P*), expressed in 100%, are also listed in Table 2. These values are roughly approximate because equations (2) and (3) assume that the decrease in the elastic modulus is fully due to the existence of porosity and neglect cracking, residual stress or surface roughness effects, which are also present in our case. Therefore, *P*(%) values are probably overestimated, particularly for samples with a large amorphous fraction. Note also that the Young's modulus of amorphous molybdenum oxides is probably lower than that of their crystalline counterparts, as observed in other systems [48].

3.4. Preparation of ordered arrays of molybdenum oxide submicrometer structures and their mechanical properties

Following films preparation, attempts were made to fabricate ordered arrays of molybdenum oxide submicrometer structures on e-beam patterned Au/Ti/Si substrates from the electrolyte at pH = 9. Figure 9a shows a fabrication scheme of the molybdenum oxide submicrometer structure arrays. In order to avoid overplating, the deposition time was fixed to 25 s for an applied potential of –1.4 V. Figure 9b shows an on-top SEM image of an array of molybdenum oxide pillars (500 nm in diameter) before resist removal; the corresponding EDX mapping analyses confirmed the presence of oxygen and molybdenum elements in the cylindrical cavities. A tilted view of an array of pillars (200 nm in diameter) is shown in Figure 9c. The pillars presented good adherence to the Au surface and preserved their integrity after resist removal. The same holds for the stripes shown in figure 9d. The mechanical properties of 500 nm-thick stripes were also evaluated by nanoindentation. The results indicated that they were mechanically softer than the film analogues. Namely, H and E_r were around 0.7 and 13 GPa, respectively, for stripes up to 2 μm in width. This is probably due to the enhanced surface roughness of the patterned structures as compared to the continuous films. H and E_r values of wider stripes tend to be larger, approaching the values of the films.

4. Conclusions

Molybdenum oxide films with varying morphology, crystallographic structure, and mechanical properties have been obtained potentiostatically onto glass/ITO substrates. Such tuning of properties has been accomplished by simply changing the pH of the electrolyte and through the addition of a cationic surfactant (CTAB) to the bath. CTAB not only improves the adherence of the films and reduces the cracking phenomena, but also increases films' crystallinity and brings about changes in the distribution of molybdenum oxidation states. The mechanical properties of the films produced from

CTAB-containing baths are also enhanced. Finally, the successful growth of crack-free, well-defined, ordered arrays of molybdenum oxide structures onto submicrometer patterned pillar and stripe motifs is demonstrated and the resulting mechanical properties assessed.

Acknowedgements

This work has been partially funded by 2014-SGR-1015 from *Generalitat de Catalunya* and MAT2011-27380-C02-01 project and CTS-11/07 (*Acceso Sala Blanca CT-ISOM, Infraestructuras Científicas y Tecnológicas Singulares*) from Spanish *Ministerio de Economía y Competitividad* (MINECO). E. Pellicer is grateful to MINECO for the 'Ramón y Cajal' contract (RYC-2012-10839). M. Guerrero acknowledges the support of the Secretary for Universities and Research of the Government of Catalonia and the COFUND Programme of the Marie Curie Actions of the 7th R&D Framework Programme of the European Union for the 'Beatriu de Pinos' contract (2013 BP-B 00077). M. D. Baró acknowledges partial financial support from an ICREA-Academia Award.

References

[1] N. A. Chernova, M. Roppolo, A.C. Dillon, M.S. Whittingham,;1; Layered vanadium and molybdenum oxides: batteries and electrochromics, J. Mater. Chem. 19 (2009) 2526-2552. .

[2] M.-J. Lee, S.I. Kim, C.B. Lee, H. Yin, S.-E. Ahn, B.S. Kang, K.H. Kim, J.C. Park, C.J. Kim, I. Song, S.W. Kim, G. Stefanovich, J.H. Lee, S.J. Chung, Y.H. Kim, Y. Park,;1; Low-temperature-grown transition metal oxide based storage materials and oxide transistors for high-density non-volatile memory, Adv. Funct. Mater. 19 (2009) 1587-1593.

[3] V. S. Saji, C.W. Lee,;1; Molybdenum, molybdenum oxides, and their electrochemistry, ChemSusChem 5 (2012) 1146-1161.

[4] B. Hu, L. Mai, W. Chen, F. Yang,;1; From MoO_3 nanobelts to MoO_2 nanorods: Structure transformation and electrical transport, ACS Nano 3 (2009) 478-82. .

[5] Y. Shi, B. Guo, S.A. Corr, Q. Shi, Y.S. Hu, K.R. Heier, L. Chen, R. Seshadri, G.D. Stucky,;1; Ordered mesoporous metallic MoO_2 materials with highly reversible lithium storage capacity, Nano Letters 9 (2009) 4215-4220. .

[5] C. A. Ellefson, O. Marin-Flores, S. Ha, M.G. Norton,;1; Synthesis and applications of molybdenum (IV) oxide, J. Mater. Sci. 47 (2012) 2057–2071.

[6] O. Marin-Flores, T. Turba, C. Ellefson, K. Wang, J. Breit, J. Ahn, M.G. Norton, S. Ha,;1; Nanoparticle molybdenum dioxide: A highly active catalyst for partial oxidation of aviation fuels, Appl. Catal. B: Environ. 98 (2010) 186-192.

[7] L. Q. Mai, B. Hu, W. Chen, Y.Y. Qi, C.S. Lao, R.S. Yang, Y. Dai, Z.L. Wang,;1; Lithiated MoO_3 nanobelts with greatly improved performance for lithium batteries, Adv. Mater. 19 (2007) 3712-3716.

[8] T. He, Y. Ma, Y. Cao, P. Jiang, X. Zhang, W. Yang, J. Yao,;1; Enhancement effect of gold nanoparticles on the UV-light photochromism of molybdenum trioxide thin films, Langmuir 17 (2001) 8024-8027. .

[9] T. He, J. Yao,;1; Photochromism of molybdenum oxide, Photochem. Photobiol. C: Photochem. Rev. 4 (2003) 125-143.

[10] G. Beydaghyan, S. Dorion, A. Haché, P.V. Ashrit,;1; Enhanced photochromism in nanostructured molybdenum trioxide films, Appl. Phys. Lett. 95 (2009) 051917.

[11] R.S. Patil, M.D. Uplane, P.S. Patil,;1; Structural and optical properties of electrodeposited molybdenum oxide thin films, Appl. Surf. Sci. 252 (2006) 8050-8056.

[12] J. Scarminio, A. Lourenço, A. Gorenstein,;1; Electrochromism and photochromism in amorphous molybdenum oxide films, Thin Solid Films 302 (1997) 66-70. .

[13] K. A. Gesheva, T. Ivanova, F. Hamelmann,;1; Optical coatings of CVD-transition metal oxides as functional layers in “smart windows” and X-ray mirrors, J. Opt. Elect. Adv. Mater. 7 (2005) 1243-1252.

[14] L. Tian, L. Liu, L. Chen, N. Lu, H. Xu,;1; Fabrication of amorphous mixed-valent molybdenum oxide film electrodeposited on a glassy carbon electrode and its application as a electrochemistry sensor of iodate, Sens. Actuators B Chem. 105 (2005) 484-489.

[15] C. Imawan, H. Steffes, F. Solzbacher, E. Obermeier,;1; A new preparation method for sputtered MoO_3 multilayers for the application in gas sensors, Sens. Actuator B Chem. B 78 (2001) 119-125.

[16] A. M. Taurino, A. Forleo, L. Francioso, P. Siciliano, M. Stalder, R. Nesper,;1; Synthesis, electrical characterization, and gas sensing properties of molybdenum oxide nanorods, Appl. Phys. Lett. 88 (2006) 152111. .

[17] B. Mendoza-Sánchez, T. Brousse, C. Ramírez-Castro, V. Nicolosi, P.S. Grant,;1; An investigation of nanostructured thin film α-MoO_3 based supercapacitor electrodes in aqueous solution, Electrochim. Acta 91 (2013) 253–260.

[18] S. S. Sunu, E. Prabhu, V. Jayaraman, K.I. Gnanasekar, T. Gnanasekaran,;1; Gas sensing properties of PLD made MoO_3 films, Sens. Actuators B Chem. 94 (2003) 189-196.

[19] T. Ivanova, A. Szekeres, M. Gartner, D. Gogova, K.A. Gesheva,;1; Spectroscopic characterization of CVD-molybdenum oxide films, Electrochim. Acta 46 (2001) 2215-2219.

[20] A. F. Jankowski, L.R. Schrawyer,;1; Reactive sputtering of molybdenum, Thin Solid Films 193-194 (1990) 61-71.

[21] G.-G. Allogho, P.V. Ashrit,;1; Wettability and photochromic behavior of molybdenum oxide thin films, Thin Solid Films 520 (2012) 2326-2330.

[22] H. M. Martínez, J. Torres, M.E. Rodríguez-García, L.D. López-Carreño,;1; Gas sensing properties of nanostructured MoO_3 thin films prepared by spray pyrolysis, Phys. B 407 (2012) 3199-3202.

[23] D. Sinkeviciute, J. Batrusaitis, N. Dukstiene,;1; Layered molybdenum oxide thin films electrodeposited from sodium citrate electrolyte solution, J. Solid State Electrochem. 15 (2011) 711-723. .

[24] D. D. Yao, J.Z. Ou, K. Latham, S. Zhuiykov, A.P. O'Mullane, K. Kalantar-zadeh,;1; Electrodeposited α- and β-phase MoO_3 films and investigation of their gasochromic properties, Cryst. Growth Design 12 (2012) 1865-1870.

[25] A. G. Gad-Allah, H.A. Abd El-Rahman,;1; Evidence for anodization kinetics of molybdenum as a valve metal in buffer solutions of pH 9.3, J. Appl. Electrochem. 18 (1998) 312-313.

[26] A. K. Prasad, D.J. Kubinski, P.I. Gouma,;1; Comparison of sol–gel and ion beam deposited MoO_3 thin film gas sensors for selective ammonia detection, Sens. Actuators B Chem. 93 (2003) 25-30.

[27] T. M. McEvoy, K.J. Stevenson,;1; Electrochemical Preparation of Molybdenum Trioxide Thin Films: Effect of sintering on electrochromic and electroinsertion properties, Langmuir 19 (2003) 4316–4326.

[28] T. M. McEvoy, K.J. Stevenson,;1; Electrochemical quartz crystal microbalance study of the electrodeposition mechanism of molybdenum oxide thin films from peroxo-polymolybdate solution, Anal. Chim. Acta 496 (2003) 39-51.

[29] T. M. McEvoy, K.J. Stevenson,;1; Elucidation of the electrodeposition mechanism of molybdenum oxide from iso- and peroxo-polymolybdate solutions, J. Mater. Res. 19 (2004) 429-438.

[30] E. Gómez, E. Pellicer, E. Vallés,;1; Intermediate molybdenum oxides involved in binary and ternary induced electrodeposition, J. Electroanal. Chem. 580 (2005) 238-244.

[31] M. Gacicuta, Y. Boutaleb, L. Cattin, S.Y. Abe, Y. Lare, G. Soto, G. Louarn, M. Morsli, R. Rehamnia, M.A. del Valle, A. Drici, J.C. Bernède,;1; Electrochemical preparation of MoO_3 buffer layer deposited onto the anode in organic solar cells, Phys. Status Solidi A 207 (2010) 1905-1911. .

[32] A. Guerfi, R.W. Paynter, L.H. Dao,;1; Characterization and Stability of Electrochromic MoO_3 Thin Films Prepared by Electrodeposition, J. Electrochem. Soc. 142 (1995) 3457-3464.

[33] M. A. Malik, M.A. Hashim, F. Nabi, S.A. AL-Thabaiti, Z. Khan,;1; Anti-corrosion ability of surfactants: A review, Int. J. Electrochem. Sci. 6 (2011) 1927–1948. .

[34] B. M. Praveen, T.V. Venkatesha,;1; New brightener for Zn-Fe alloy plating from sulphate bath, Int. J. Electrochem. (2011) 132138.

[35] M.-S. Wu, M.-J. Wang,;1; Nickel oxide film with open macropores fabricated by surfactant-assisted anodic deposition for high capacitance supercapacitors, Chem. Commun. 46 (2010) 6968-6970.

[36] Y. S. Kim, J.K. Lee, J.H. Ahn, E.K. Park, G.P. Kim, S.H. Baeck,;1; Fabrication of mesoporous cerium dioxide films by cathodic electrodeposition, J. Nanosci. Nanotechnol. 7 (2007) 4198-201.

[37] V. Nirupama, M.C. Sekhar, T. Subramanyam, S. Uthanna,;1; Structural and electrical characterization of magnetron sputtered MoO_3 thin films, J. Phys. Conf. Ser. 208 (2010) 012101.

[38] L. Silipigni, F. Barreca, E. Fazio, F. Neri, T. Spanò, S. Piazza, C. Sunseri, R. Inguanta,;1; Template electrochemical growth and properties of Mo oxide nanostructures, J. Phys. Chem. C 118 (2014) 22299-22308.

[39] A. Varea, S. Pané, S. Gerstl, M.A. Zeeshan, B. Özkale, B.J. Nelson, S. Suriñach, M.D. Baró, J. Nogués, J. Sort, E. Pellicer,;1; Ordered arrays of ferromagnetic, compositionally-graded $Cu_{1-x}Ni_x$ alloy nanopillars prepared by template-assisted electrodeposition, J. Mater. Chem. C 1 (2013) 7215-7221.

[40] M. Repoux,;1; Comparison of background removal methods for XPS, Surf. Interf. Anal. 18 (1992) 567–570. .

[41] ;1;http://srdata.nist.gov/xps/.

[42] W. C. Oliver, G.M. Pharr,;1; An improved technique for determining hardness and elastic modulus using load and displacement sensing indentation experiments, J. Mater. Res. 7 (1992) 1564-1583. .

[43] A. Phuruangrat, D.J. Ham, S. Thongtem, J.S. Lee,;1; Electrochemical hydrogen evolution over MoO_3 nanowires produced by microwave-assisted hydrothermal reaction, Electrochem. Commun. 11 (2009) 1740-1743.

[44] Z.-S. Guan, Y. Zhang, Y.-J. Lu,;1; Preparation of molybdic acid aggregates and molybdenum trioxide powder with controllable size and morphology, J. Inorg. Mater. 23 (2008) 636-640.

[45] V. M. Nagirnyi, R.D. Apostolova, E.M. Shembel,;1; Electrodeposition of molybdenum oxide and its structural characteristics, Russ. J. Appl. Electrochem. 79 (2006) 1438-1442.

[46] L. P. Bicelli, B. Bozzini, C. Mele, L. D'Urzo,;1; A review of nanostructural aspects of metal electrodeposition, Int. J. Electrochem. Soc. 3 (2008) 356-408.

[47] T. J. Morley, L. Penner, P. Schaffer, T.J. Ruth, F. Bérnard, E. Asselin,;1; The deposition of smooth metallic molybdenum from aqueous electrolytes containing molybdenum ions, Electrochem. Commun. 15 (2002) 78-80.

[48] G. Alcalá, P. Skeldon, G.E. Thompson, A.B. Mann, H. Habazaki, K. Shimizu,;1; Mechanical properties of amorphous anodic alumina and tantala films using nanoindentation, Nanotechnology 13 (2002) 451–455.

[49] R. El-Mallawany,;1; Tellurite glasses. Part 1. Elastic properties, Mater. Chem. Phys. 53 (1998) 93-120.

[50] L. May, F. Yang, Y. Zhao, X. Xu, L. Xu, B. Hu, Y. Luo, H. Liu,;1; Molybdenum oxide nanowires: synthesis & properties, Mater. Today 14 (2011) 346-353.

[51] N. Ramakrishnan, V.S. Arunachalam,;1; Effective elastic moduli of porous solids, J. Mater. Res. 25 (1990) 3930–3937.

[52] X. Y. Sun, G.K. Xu, X. Li, X.L. Feng, H. Gao,;1; Mechanical properties and scaling laws of nanoporous gold, J. Appl. Phys. 113 (2013) 023505.

Figure captions

Figure 1 Cyclic voltammetries recorded from 0.2 M Na_2MoO_4 ("no add") and 0.2 M Na_2MoO_4 + 0.01 M CTAB ("CTAB") electrolytes at pH = 1, pH = 6 and pH = 9. Scan rate: 50 mV s^{-1}.

Figure 2 *j*-t curves recorded during the potentiostatic deposition of molybdenum oxide films from 0.2 M Na_2MoO_4 ("no add") and 0.2 M Na_2MoO_4 + 0.01 M CTAB ("CTAB") electrolytes at pH = 1 (–0.9 V), pH = 6 (–1.4 V), and pH = 9 (–1.4 V). The inset shows a zoomed detail of the curves during the first stages of deposition.

Figure 3 SEM images of molybdenum oxide films grown on ITO/glass substrates at (a) pH = 1 "no add" bath, Q = 4.8 C cm^{-2}; (b) pH = 6 "no add" bath, Q = 711 mC cm^{-2}; (c) pH = 6 "CTAB" bath, Q = 426 mC cm^{-2}; (d) pH = 9 "no add" bath, Q = 400 mC cm^{-2}; and (e) pH = 9 "CTAB" bath, Q = 593 mC cm^{-2}.

Figure 4 XRD patterns of molybdenum oxide films grown on ITO/glass substrates at (a) pH = 1 without CTAB in the bath, (b) pH = 6 and (c) pH = 9 without (no add) and with CTAB in the bath.

Figure 5 HRTEM images of molybdenum oxide films obtained by (a) CTAB-free bath at pH = 6, (c) CTAB-free bath at pH = 9 and (e) CTAB-containing bath at pH = 9. (b, d and f) are the corresponding SAED patterns.

Figure 6 Experimental and deconvoluted Mo 3d XPS bands corresponding to molybdenum oxide films produced in CTAB-free baths at (a) pH = 1, (b) pH = 6 and (c) pH = 9.

Figure 7 Experimental and deconvoluted Mo 3d XPS bands corresponding to molybdenum oxide films produced in CTAB-containing baths at (a) pH = 6 and (b) pH = 9.

Figure 8 Load-unload indentation curves of the molybdenum oxide films grown on glass/ITO substrates.

Figure 9 (a) Schematic picture of the fabrication of arrays of molybdenum oxide pillars and stripes on e-beam lithographed Si/Ti/Au substrates. (b) On-top SEM image of molybdenum oxide pillars (left) and corresponding EDX mapping (right) before resist removal. (c) and (d) 70º tilted SEM images of arrays of molybdenum oxide pillars (200 nm in diameter) and stripes (1 μm x 15 μm), respectively. The inset of Figure 9d shows narrower stripes of 100 nm width (scale bar is 200 nm). The submicrometer structures were grown from CTAB-free bath at pH = 9 at E = –1.4 V for 25 s (ω = 100 rpm). Note that the previously evaporated Au layer showed some growth defects in the form of protrusions as indicated with an arrow in Figure 9d.

Tables

Table 1. Binding energy (in eV) for the $3d_{3/2}$ and $3d_{5/2}$ doublets of Mo 3d XPS core-level spectra obtained from the deconvolution of experimental curves shown in Figure 6 (films obtained from CTAB-free electrolyte)

	Binding energy (eV)							
Sample	Mo^{6+}		Mo^{5+}		Mo^{4+}		Mo^{0}	
(no add)	3/2	5/2	3/2	5/2	3/2	5/2	3/2	5/2
pH = 1	236.9	232.0	235.8	232.8	234.3	*	231.1	*
pH = 6	236.8	232.3	235.5	233.0	234.6	*	231.0	*
pH = 9	236.6	231.7	234.9	232.9	234.2	229.8	231.0	228.2

*of very low intensity (nearly negligible contribution)

Table 2. Values of H and E_r determined from nanoindentation curves. Young's modulus, E, has been calculated assuming a Poisson's ratio of 0.28. Films' porosity has been estimated using equations (2) and (3) and considering E_{bulk} = 540 GPa [50].

Film	H (GPa)	E_r (GPa)	E (GPa)	P (%) Eq. 2	P (%) Eq. 3
pH1 no add	1.30±0.07	22.46±0.76	20.30±0.70	73	81
pH6 no add	1.67±0.04	20.24±0.38	18.33±0.35	75	82
pH6 CTAB	2.07±0.04	24.95±0.27	22.50±0.25	72	80
pH9 no add	0.67±0.04	16.36±0.47	14.86±0.43	77	83
pH9 CTAB	2.37±0.07	29.96±0.58	26.90±0.53	70	78

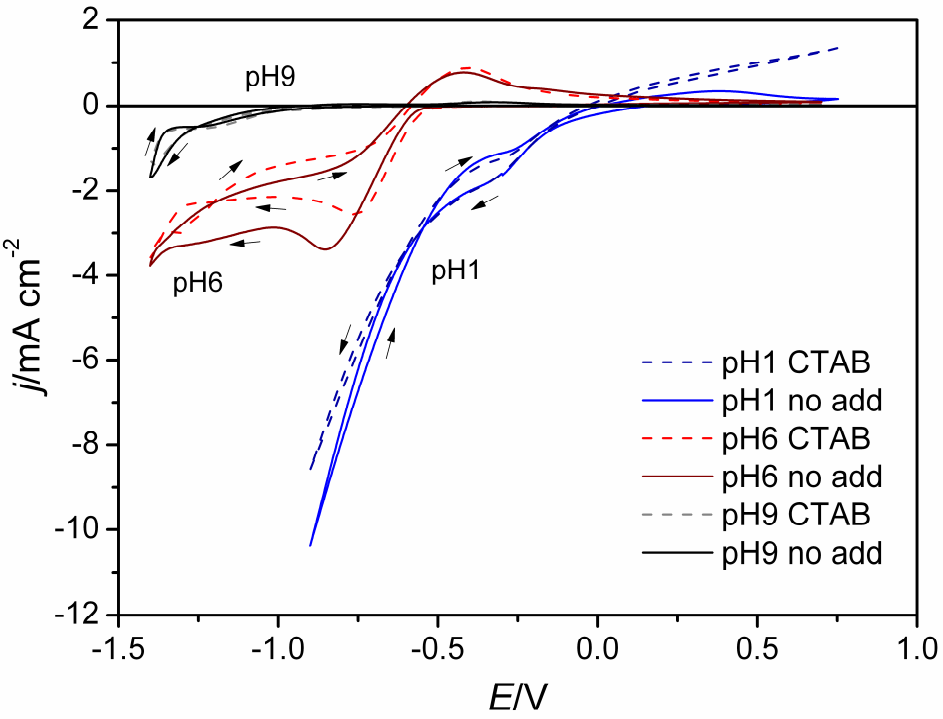

Fig. 1

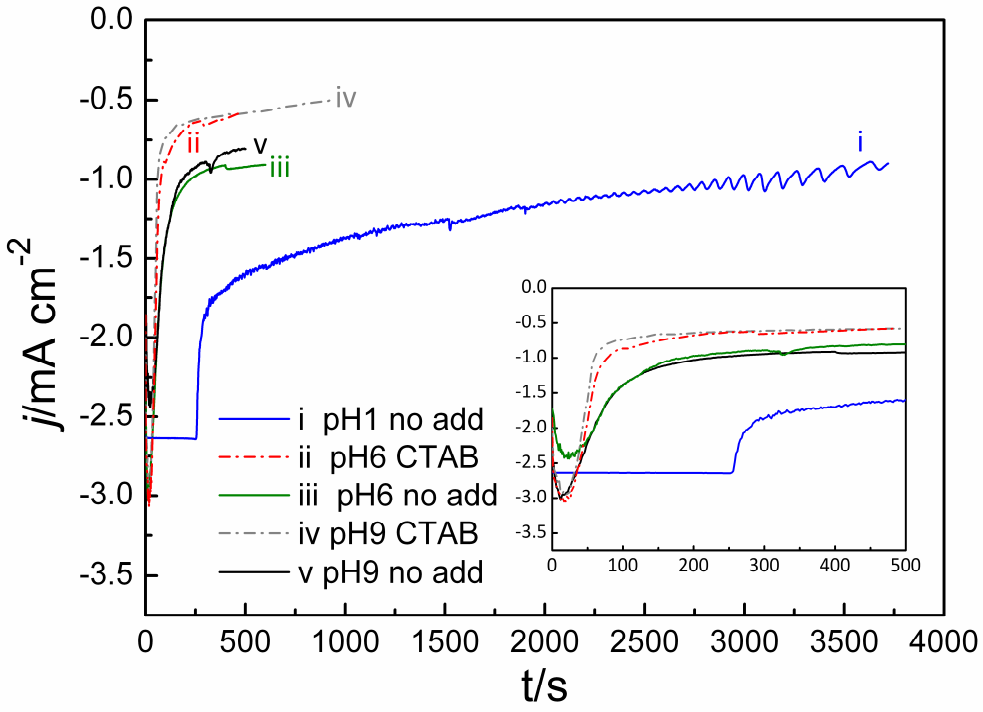

Fig. 2

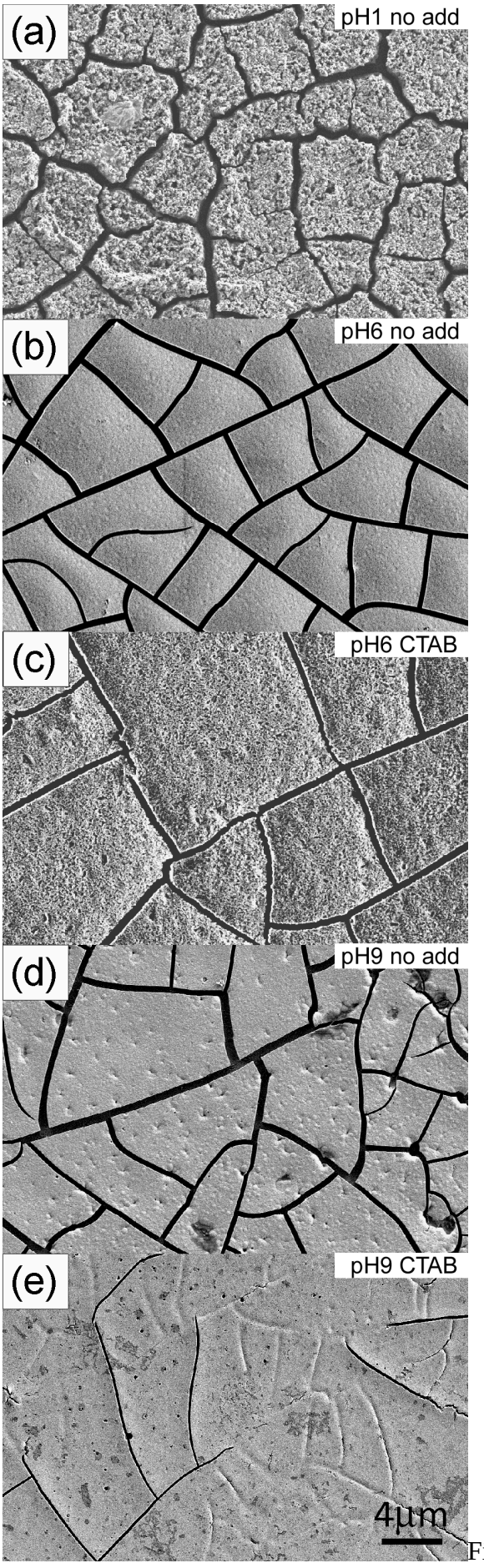

Fig. 3

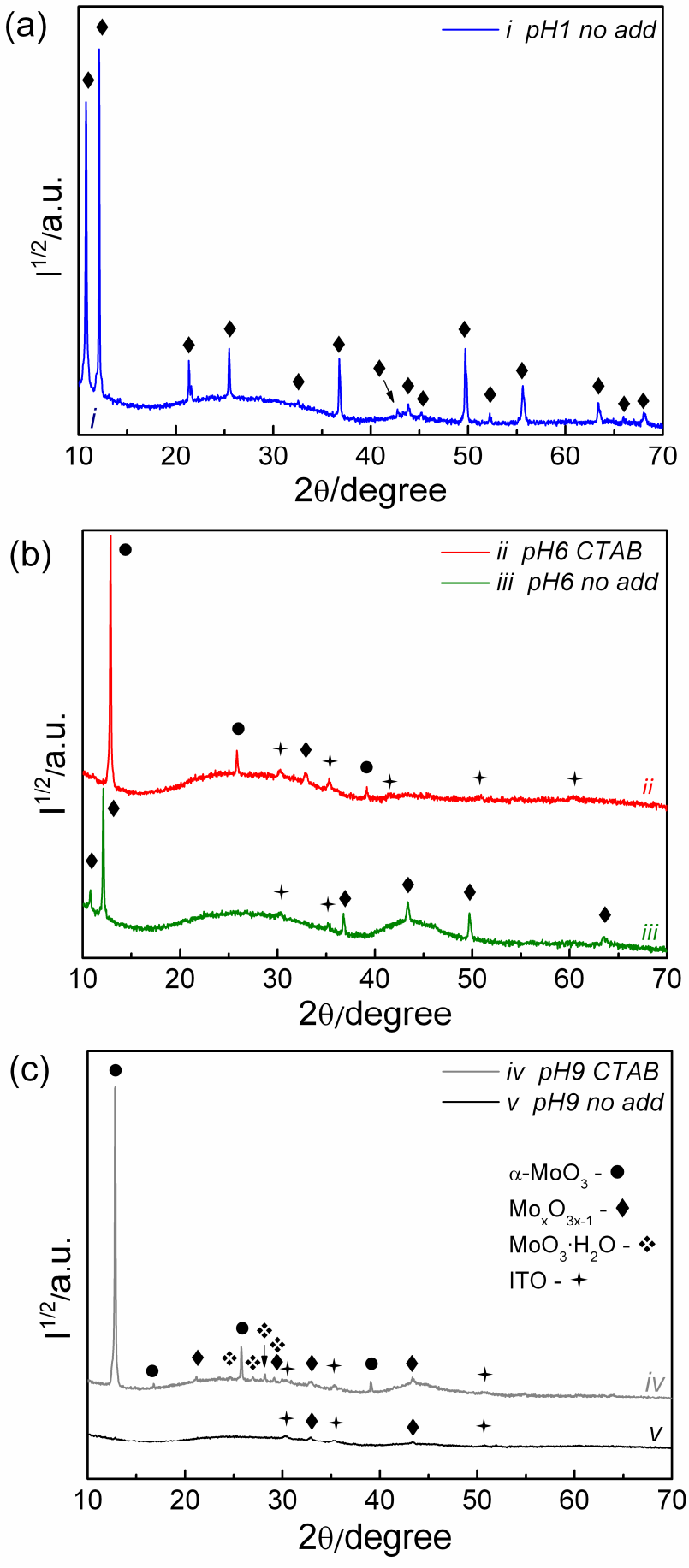

Fig. 4

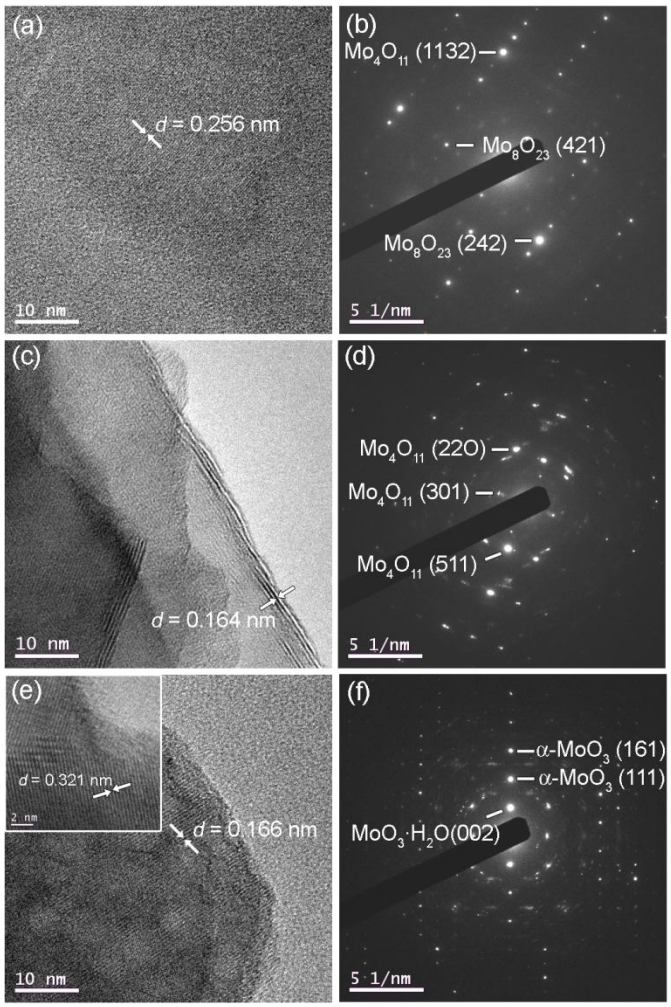

Fig. 5

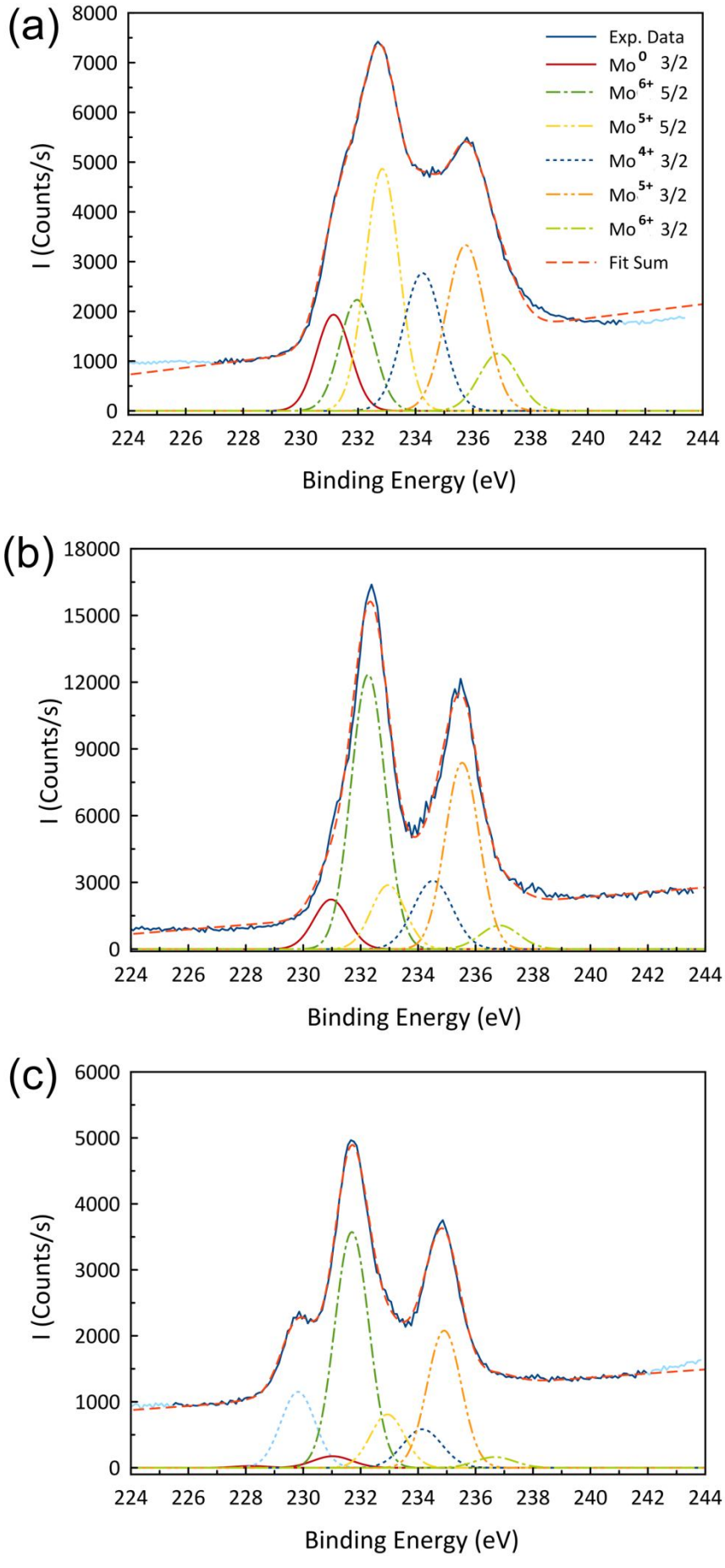

Fig. 6

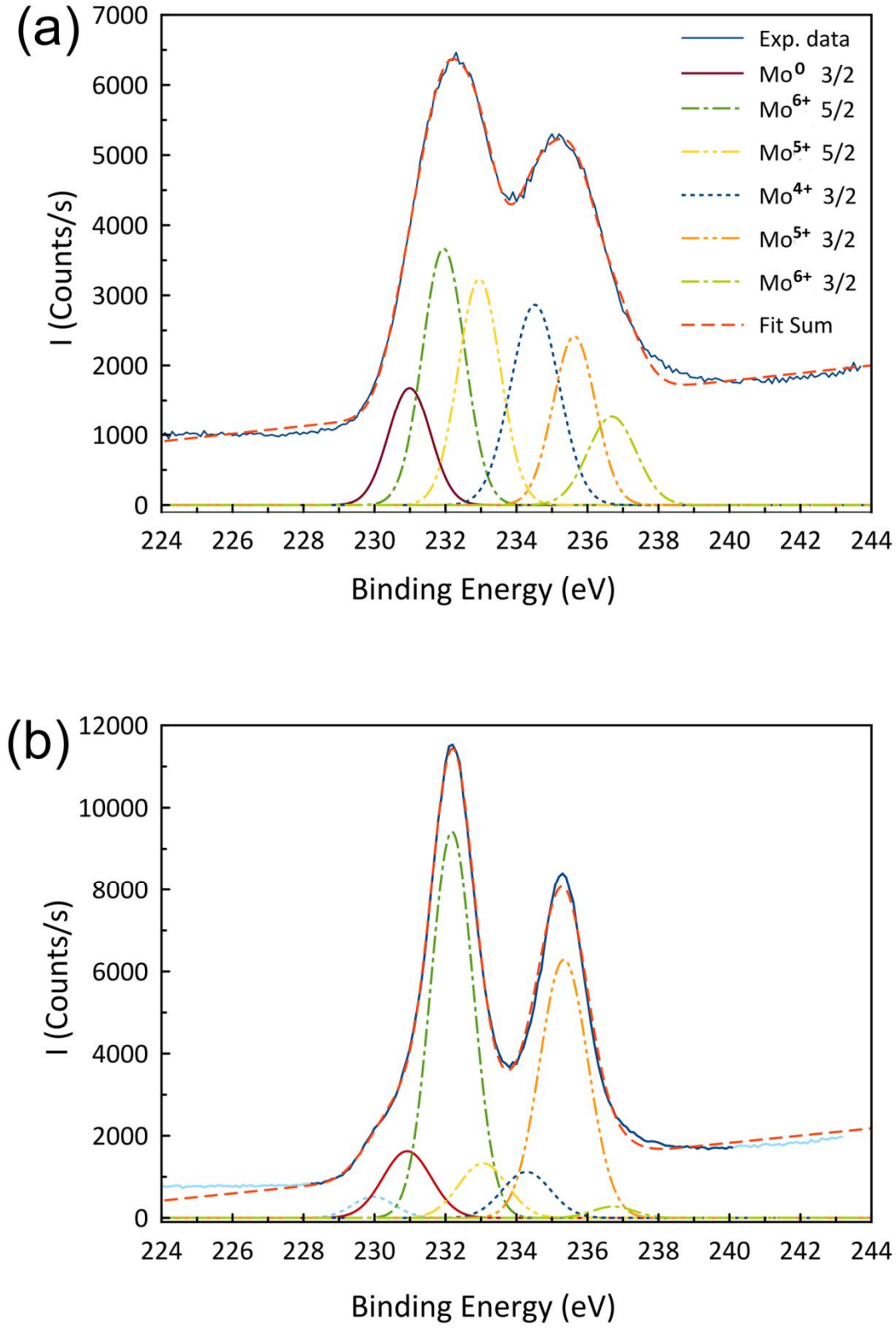

Fig. 7

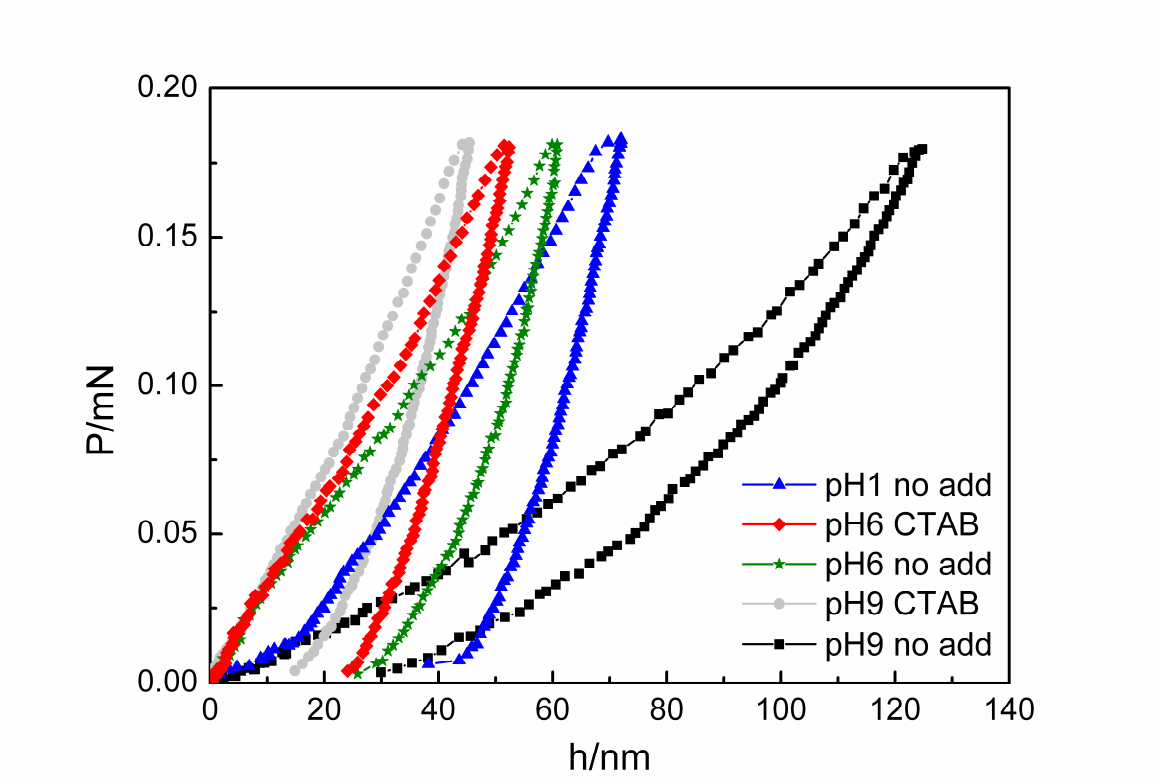

Fig. 8

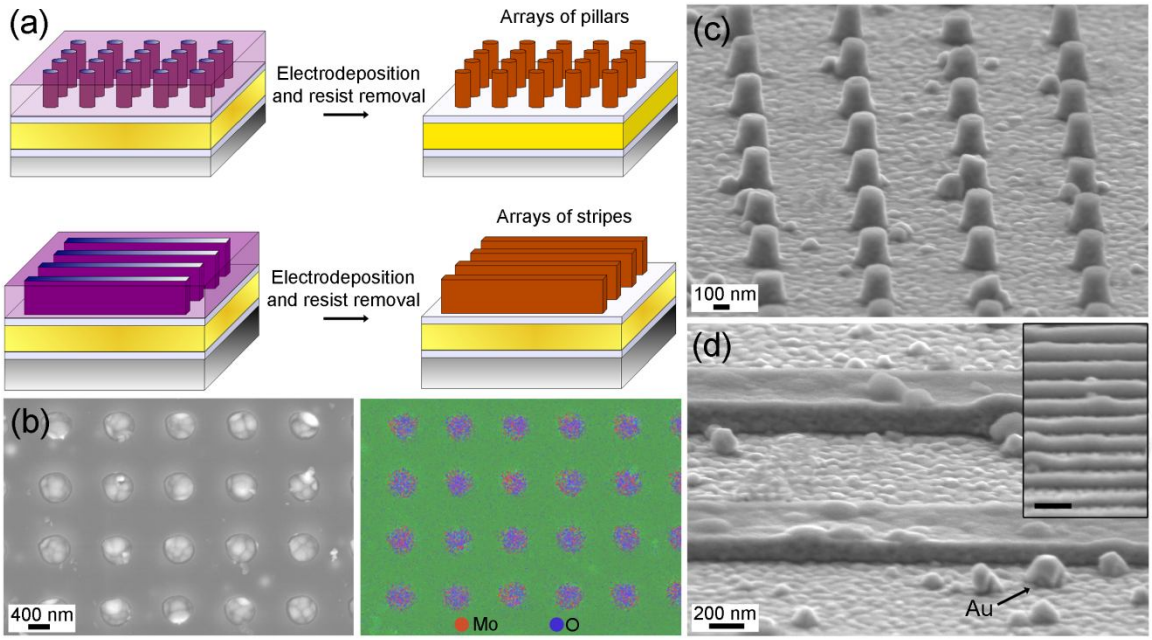

Fig. 9